LA-UR-96- 2423

CONF-960202--34

Title: TANTALUM POWDER CONSOLIDATION, MODELING AND PROPERTIES

Author(s): SHERRI A. BINGERT, MST-6
VICTOR D. VARGAS, MST-6
HASKELL C. SHEINBERG, MST-6

Submitted to: TANTALUM
1996 TMS ANNUAL MEETING
ANAHEIM, CALIFORNIA
FEBRUARY 4-8, 1996

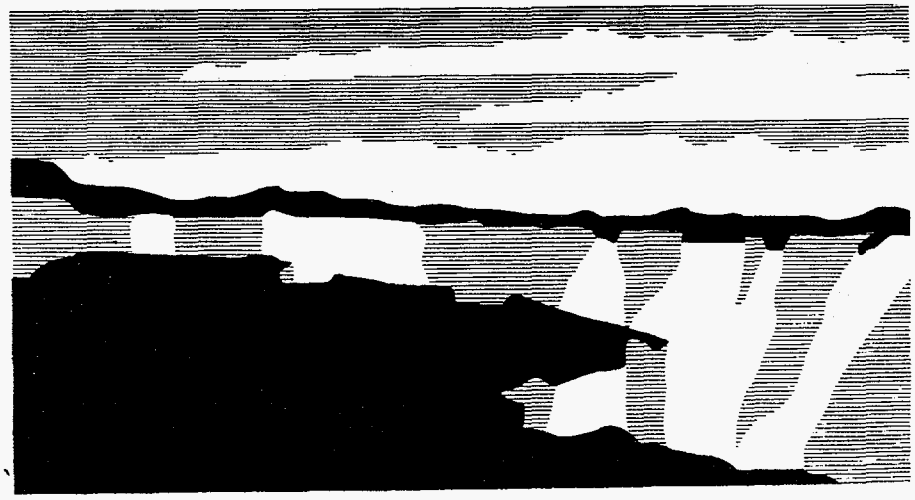

Los Alamos
NATIONAL LABORATORY

Form No. 836 R5
ST 2629 10/91

DISCLAIMER

TANTALUM POWDER CONSOLIDATION, MODELING, AND PROPERTIES

Sherri R. Bingert, Victor D. Vargas, and Haskell Sheinberg

Los Alamos National Laboratory
Los Alamos, NM 87545

Abstract

A systematic approach was taken to investigate the consolidation of tantalum powders. The effects of sinter time, temperature and ramp rate; hot isostatic pressing (HIP) temperature and time; and powder oxygen content on consolidation density, kinetics, microstructure, crystallographic texture, and mechanical properties have been evaluated. In general, higher temperatures and longer hold times resulted in higher density compacts with larger grain sizes for both sintering and HIP'ing. HIP'ed compacts were consistently higher in density than sintered products. The higher oxygen content powders resulted in finer grained, higher density HIP'ed products than the low oxygen powders. Texture analysis showed that the isostatically processed powder products demonstrated a near random texture. This resulted in isotropic properties in the final product. Mechanical testing results showed that the HIP'ed powder products had consistently higher flow stresses than conventionally produced plates, and the sintered compacts were comparable to the plate material.

A micromechanics model (Ashby HIP model) has been employed to predict the mechanisms active in the consolidation processes of cold isostatic pressing (CIP), HIP and sintering. This model also predicts the density of the end product and whether grain growth should be expected under the applied processing conditions. The model predicted the densification and mechanisms well for the higher oxygen content powder using the initial parameters. However, the model consistently underpredicted the densification of the lower oxygen content powder. Modifications to the room temperature yield strength, surface energy and diffusion terms in the model yielded closer agreement. The model predicted the grain growth observed at the higher sintering temperatures and long sinter times only after the tuning was completed.

Background

Typical cast and wrought tantalum products demonstrate structural and texture gradients through the thickness of the product. The structural gradients include variations in grain size and hardness. Quite often the presence of grain size banding is an indication of texture banding which results in non-uniform deformation response in the material.

The most pronounced evidence of this phenomenon was documented by Wright, Gray, Rollett and Beaudoin [1, 2]. These investigators discovered that a particular tantalum plate responded to through-thickness compression by forming an hourglass shape rather than the expected barreling (due to the friction between the sample and the platens). On further evaluation of the plate, they determined that the observed deformation was principally due to the existence of non-uniform texture gradients through the plate thickness. During its processing, this plate developed a predominant {111} texture at its centerline and was graded to a {100} texture at its surface. The presence of this preferred orientation resulted in easier deformation near the plate surface with little or no deformation at the plate centerline; hence the hourglass shape formation on through-thickness compressive deformation.

Rajendran and Garrett [3] also investigated the effects of anisotropy on the mechanical response of several tantalum plates displaying different textures. They determined that the different preferred orientations resulted in differing work hardening behavior for mechanical testing performed over a wide range of strain rates.

The effects of processing on the subsequent texture and deformation response of tantalum have been studied as well [4-6]. This work pointed to the root cause of the material behavior as the formation of a solidification texture during casting. This texture development was carried through the subsequent forging/rolling steps with some evolution. The final product had properties commensurate with its processing route and schedule. In addition to the work cited above, there has been much activity in recent years in attempts to thoroughly understand the effects of processing on the microstructure, texture, and ultimately the deformation response of tantalum [7, 8].

Powder processing offers the possibility of producing a uniform, randomly textured product that will avoid the non-uniform mechanical behavior evident in much of the cast/wrought tantalum plate and bar products produced

today. In this study, isostatic processing was employed in order to prepare a randomly textured product. This type of consolidation eliminates die wall friction present in conventional uniaxial pressing and minimizes non-uniform through-thickness deformation during processing.

Experimental Procedures

Powders and Consolidation

The starting powder for the conventional P/M consolidation work was commercially available, metallurgical grade, sodium-reduced powder supplied by Cabot Performance Materials. One-half of the batch was used as-received (Ta-48A), and contained a typical oxygen content for this type of powder. The second half of the batch received a reduction treatment to lower the oxygen content (Ta-48B). This allowed for a direct evaluation of the effect of oxygen content on the final properties of products manufactured by the same procedure.

Prior to the sintering and HIP studies the two powders were initially cold isostatically pressed (CIP'ed) at 345 MPa. This resulted in cylinders approximately 25.4 mm in diameter and 80% of theoretical density (ρ_{th}).

The sintering experiments were performed at 10^{-4} torr vacuum or better throughout the sintering cycle in a resistively heated tungsten-element furnace. Initially three experiments were performed at 2200, 2400 and 2600 °C with a three hour hold at temperature. The ramp up rate was fairly rapid (~37°C/min). However, it was noticed that the pressure increased in the furnace chamber at ~600°C and again in the range of 2000-2200°C. Following this result, the second set of experiments, 2400°C for hold times of 1, 3, and 5 hours, also included a slower ramp rate. In these experiments, a rate of 10°C/min to 800°C, a 30 minute hold at 800°C, and a ramp rate of ~27°C/min from 800°C to 2400°C were employed. This slower ramp rate run still resulted in some pressure increases at 600°C and 2000°C. It should also be noted that at these high operating temperatures and vacuum levels, there is significant vaporization of Ta onto the quartz window of the optical pyrometer. Therefore, the temperature measurements may be affected. In addition, the temperatures reported here have not been corrected for emissivity. In light of the above, it is probable the actual temperature in the furnace was higher than recorded. For consistency, the initial temperature measurement was taken just as the temperature stabilized for the hold. At this time, and for the future runs at the same temperature, the furnace power was controlled via a Watt transducer.

HIP experiments were performed on the CIP'ed compacts (contained in evacuated, electron-beam welded Ta cans) at 207 MPa. The temperature was varied from 1400°C to 1800°C with a constant one hour hold time at temperature. Temperature and pressure were ramped up simultaneously over four hours. A kinetics study was also performed at 1400°C, 207 MPa and hold times ranging from fifteen minutes to four hours.

All compacts were examined using standard metallographic preparation techniques and light microscopy. Vickers microhardness was determined using 500 gram loads, according to ASTM specification E384-84 [9]. Grain size was determined by the Abrams three-circle method, ASTM E112-85 [10]. Densities were determined using the Archimedes Principle method. Bulk texture measurements were performed by neutron diffraction techniques, and verified by microtexture analysis using orientation imaging microscopy.

Mechanical tests included compression testing at a variety of strain rates on Instron and Split-Hopkinson bar machines.

Modeling

The Ashby HIP model [11] was used in this study to predict the active, dominant mechanisms during the consolidation process. In order to accomplish this end, a wide variety of data was entered into the model. The starting data is given in Table I. The information contained in this table comes from two principal sources [12, 13] and some is initially assumed by the program.

The maps for CIP, sinter, and HIP were all determined for the conditions in Table I. The model was "tuned' first for the CIP map and then for sintering using the experimental data.

Results and Discussion

The powders were thoroughly characterized prior to consolidation. The chemical analyses and powder characteristics are listed in Table II. The two powder batches were determined to be essentially identical with the exception of the chemistries; the principal difference between these powders was the oxygen and hydrogen contents. The reduction process resulted in an increase in the hydrogen content for Ta-48B. Oxygen content was expected to have some effect on the sintering behavior and grain growth of the compacts, as well as the mechanical response. The consolidation of the powders included studies of cold isostatic pressing, sintering behavior, and hot isostatic pressing.

Sintering Study

The pressure rises observed at 600°C and 2000-2200°C during the temperature ramp up were consistent with results reported in the literature [14]. The pressure rise at 600°C was likely due to the evolution of hydrogen from within the compact, while that seen in the range of 2000-2200°C was

due to the dissociation and vaporization of tantalum oxide. The results of the sintering study are presented in figures 1 and 2, with the relative densities of the compacts plotted versus temperature and hold time, respectively. Figure 1 shows the effect of sinter temperature on the densification of the two powders. As expected, both powders increased significantly in density as the temperature was increased for a constant hold time, achieving up to 95% of theoretical density. A similar effect was observed for increasing times at temperature, as shown in figure 2. Densities up to 97% of theoretical were measured for the low oxygen content compacts.

Table I. Initial Tantalum Material Properties for the Ashby HIP Model

General Properties	
Structure Type	bcc
Solid Density	16600 kg/m^3
Melting Point	3287 K
Atomic or Molecular Weight	180.95 kg/kmol
Weighted atom-volume	1.81X10^{-29} m^3/atom
Surface Energy	2.68 J/m^2
Mechanical Properties	
Young's Modulus (@R.T.)	191.92 GPa
Yield Stress (@R.T.)	137.8 MPa
T Dependence of Yield	0.5
Power-Law Creep Exponent	4.00
Reference Stress (P-L Creep)	68.9 MPa
Activation Energy (P-L Creep)	491.91 kJ/mol
Low T to High T creep transition T	1643.5 K
C for Low T Creep (Q-ltc=C*Qc)	0.65
Diffusion Properties	
Pre-exp. Volume Diffusion	1.0X10^{-4} m^2/s
Activation Energy (Vol. Diff.)	491.91 kJ/mol
Pre-exp. Boundary Diffusion	2.63X10^{-14} m^3/s
Activation Energy (Bdry. Diff.)	295.14 kJ/mol
Grain Growth	
Pre-exp. Surface Diffusion	7.88X10^{-10} m^3/s
Activation Energy (Surf. Diff.)	491.91 kJ/mol
Pre-exp. Boundary Mobility	1.31X10^{-14} m^3/s
Activation Energy (Bdry. Mobil.)	393.52 kJ/mol
Particle Characteristics	
Particle Radius	9.0X10^{-6} m
Ratio of Radii (R_{max}/R_{mean})	2
Grain Diameter in Particle	1.8X10^{-5} m

Table II. Tantalum Powder Characteristics

	Ta-48A	Ta-48B
Fisher Avg Particle Size	9.5μm	9.9μm
Bulk Density	22% ρ_{th}	23% ρ_{th}
Tap Density	34% ρ_{th}	35% ρ_{th}
Size - Elzone (median)	18.3 μm	15.2 μm
O	841 ppm	234 ppm
H	22 ppm	651 ppm

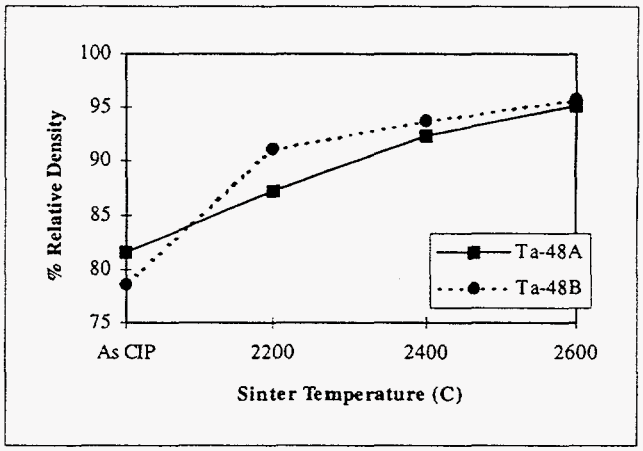

Figure 1. The effect of sintering temperature on the densification of the high and low oxygen powder compacts.

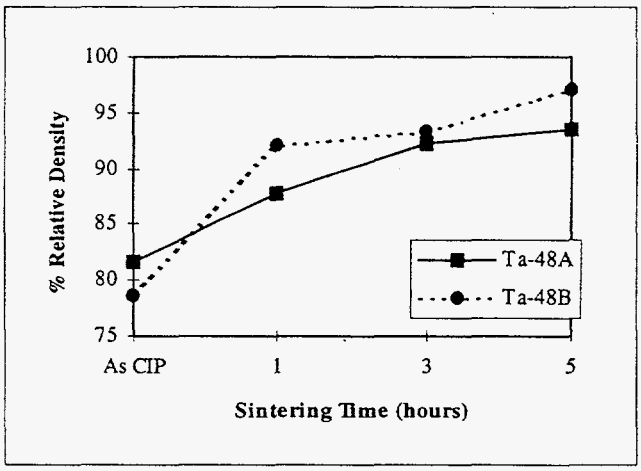

Figure 2. The effect of sintering time at 2400°C on the densification of the high and low oxygen powder compacts.

In general, the high oxygen content compacts demonstrated higher hardness and finer grain size than the lower oxygen content material. In addition to these results, it was observed that both powders exhibited significant grain growth during sintering. Also, as the temperature and hold times were increased, the grain growth was even more pronounced, with the average grain size increasing from ~20 μm at 2200°C to over 40 μm at 2600°C. Grain size

increased with time at 2400°C from ~20 μm at one hour hold up to ~40 μm for a five hour hold.

Microstructures illustrating the effects of sintering time on grain size, pore location, and pore morphology are shown in figure 3. It is evident from these micrographs that at shorter sintering times, the pores are situated along the grain boundaries with a few spherical pores in the grain interiors. At longer sintering times (or higher temperatures) there are more pores trapped intragranularly as the grain boundaries have migrated past the pores prior to the pores closing. Additionally, note the morphology of the pore indicated in figure 3b. The concave shape of the pore interior produces a high energy surface, thus the rate of pore closure is retarded due to its unfavorable morphology. This allows grain boundary migration to occur, trapping the pores within grain interiors.

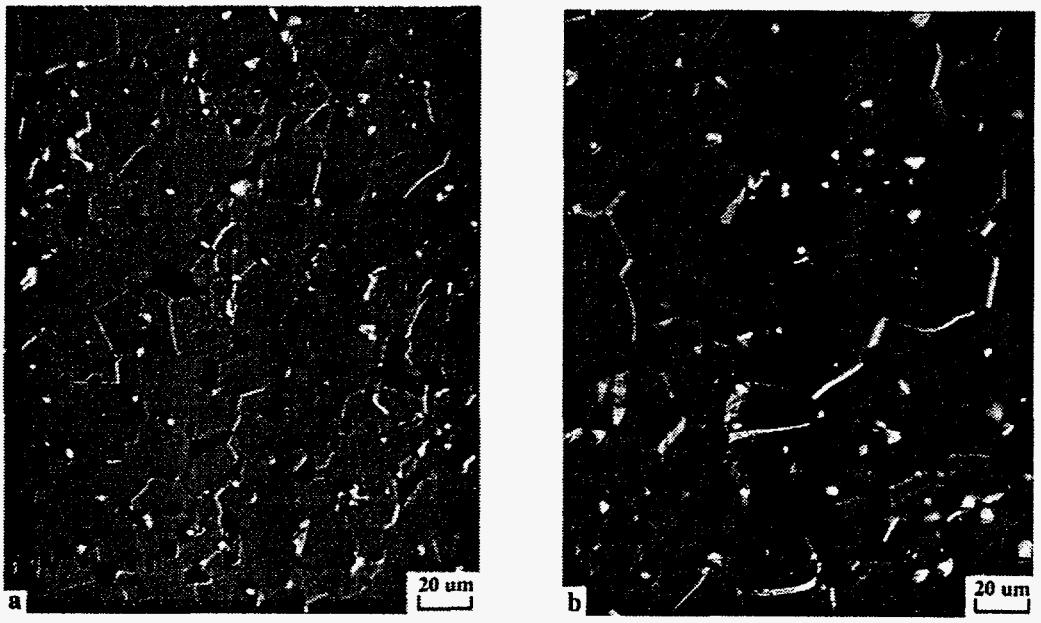

Figure 3. Light micrographs of a) Ta powder compact sintered at 2400°C for one hour and b) Ta compact sintered at 2400°C for 5 hours.

Hot Isostatic Pressing Study

The HIP'ing study was successful at producing near fully dense compacts, especially in the case of the higher oxygen content powders as illustrated in figure 4. At a HIP temperature of 1400°C, a fully dense compact was achieved for the high oxygen content powder. The low oxygen powder compacts consistently demonstrate 95% ρ_{th} or better. The density reached a plateau of approximately 98% in this case. A kinetics study performed at 1400°C for hold times ranging from fifteen minutes to two hours showed that all compacts densified to above 99% ρ_{th}, with only a slight increase in relative density as hold time increased.

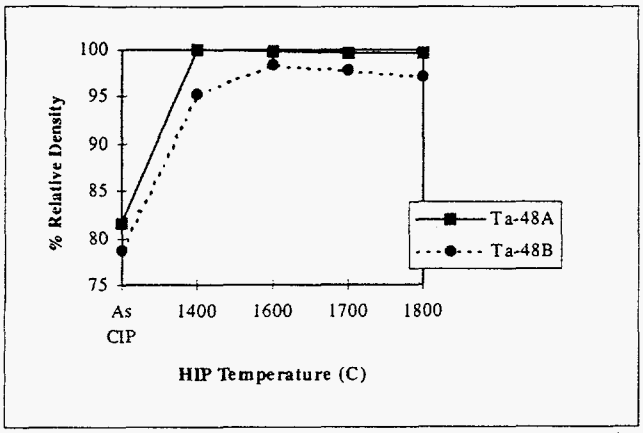

Figure 4. The influence of HIP temperature on the density of both the high and low oxygen content powders.

The microstructure exhibited a uniform equiaxed structure with an extremely fine pore distribution. Figure 5 shows a typical microstructure for the HIP'ed Ta powder. While the hardness remained constant for all HIP conditions, the grain size increased with increasing temperature and hold time. This grain coarsening was consistent with the results seen previously in the sintering section. Again, the grain boundary motion occurred readily and trapped pores prior to closure. Aiding this effect was the fact that in the HIP process, the compacts were in a closed can (i.e. gases cannot evolve). The high oxygen powder probably had oxygen present on prior particle surfaces which would later pin the boundaries and restrict grain boundary migration, thus the pores may close prior to grain growth occurring. The low oxygen powder, in contrast, did not have these barriers to grain boundary motion, and thus allowed pores to be trapped intragranularly.

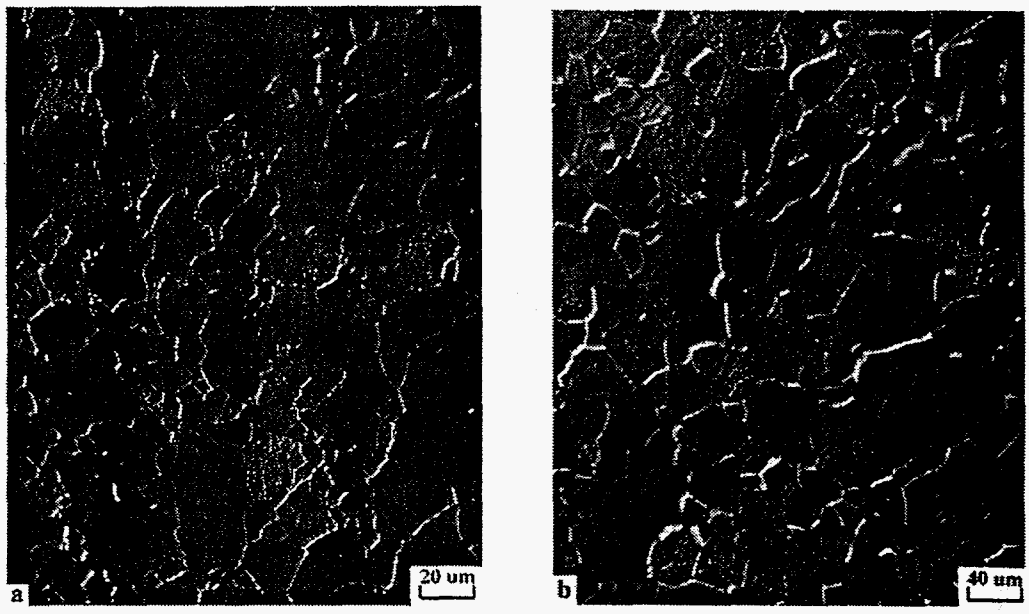

Figure 5. Light micrographs of high oxygen content compacts HIP'ed at a) 1400°C and b) 1700°C illustrating the dense, equiaxed microstructure and grain growth evident at higher temperature.

Mechanical Properties

Based on the test results to date, the powder metallurgy products in the HIP'ed conditions demonstrated significantly higher yield strengths than conventional wrought plate, while the strain hardening rate has remained consistent with the rolled plate. Figure 6 shows the results of compression tests conducted at room temperature and at a variety of strain rates for high and low oxygen powder compacts HIP'ed at 1600 and 1800 °C compared to similar strain rates for wrought product (Ta-DD). The sintered products demonstrated mechanical properties comparable to the wrought plate.

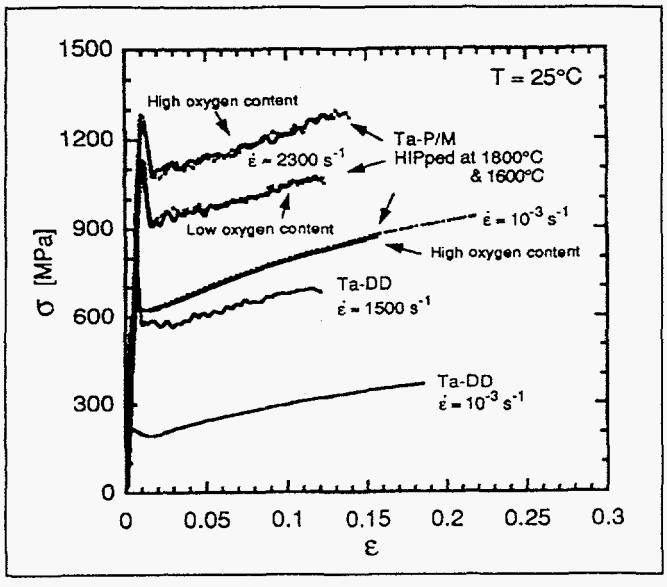

Figure 6. Results of room temperature compression tests from P/M and wrought Ta over a range of strain rates.

Texture Analysis

The HIP'ed Ta compacts displayed a near random texture as shown in figure 7. This result indicates that the isostatic processing used to fabricate these compacts has successfully produced a textureless Ta product, from which consistent and isotropic mechanical properties are expected.

Modeling

The Ashby modeling results using the data initially entered, as discussed in the Experimental Procedures section, is shown below. Figure 8 illustrates that the model was not far off in predicting the pressure density curve for cold isostatic pressing of these powders, although only one data point is represented. The model was tuned by adjusting the yield strength of the material. It may be anticipated that the yield strength of a powder should be higher than the yield strength of the same material in a conventional bulk form. By adjusting the yield strength entered in the model from 138.7 MPa to 210 MPa, the pressure density curve agreed better with the experimental data, as shown in figure 9.

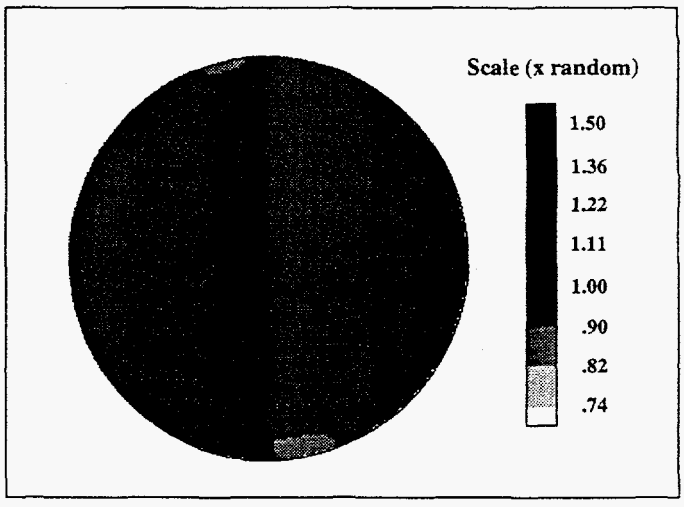

Figure 7. Neutron diffraction {001} pole figure recalculated from the orientation distribution function for HIP'ed Ta illustrating the essentially random texture.

In the case of sintering, the principal mechanisms responsible for densification are diffusion controlled. They include both grain boundary and volume diffusion. These mechanisms are both time and temperature dependent and are described by equations 1 through 4.

Stage 1 (<92%ρ_{th})
Boundary Diffusion

$$\dot{\Delta} = 43\frac{(1-\Delta_o)}{(\Delta-\Delta_o)}\frac{\delta D_b}{R^3}F_1 \qquad (1)$$

Stage 2 (>92%ρ_{th})
Boundary Diffusion

$$\dot{\Delta} = 4\frac{\delta D_b}{R^3}F_2 \qquad (2)$$

Stage 1 (<92%ρ_{th})
Volume Diffusion

$$\dot{\Delta} = 32(1-\Delta_o)\frac{D_v}{R^2}F_1 \qquad (3)$$

Stage 2 (>92%ρ_{th})
Volume Diffusion

$$\dot{\Delta} = 3\left[\frac{1-\Delta}{6\Delta}\right]^{1/3}\frac{D_v}{R^2}F_2 \qquad (4)$$

where: $\dot{\Delta}$ represents the densification rate
δD_b the boundary diffusion coefficient times the thickness
D_v the volume diffusion coefficient
R the particle radius and
F_1 and F_2 are dimensionless driving forces

principally controlled by surface energy γ.

$$F_1 = \left[(P - P_o) + 3\Delta^2 \left[\frac{2\Delta - \Delta_o}{1 - \Delta_o} \right] \frac{\gamma}{R} \right] \frac{\Omega}{kT} \qquad (5)$$

$$F_2 = \left[(P - P_1) + 2 \left[\frac{6\Delta}{1 - \Delta} \right]^{1/3} \frac{\gamma}{R} \right] \frac{\Omega}{kT} \qquad (6)$$

The terms primarily controlling the densification for both stages of sintering are δD_b, D_v, and γ. In order to tune the sinter maps, these terms were modified. Because of the interaction of these terms, the sintering predictions were not as easily adjusted as the CIP predictions. Figure 10 shows the results for the untuned model predictions of the density-temperature sinter maps for both powders. Note that the model underpredicts the densification of the low oxygen powder. This is most likely due to there being less interstitial constituents present on the particle boundaries. This results in a lower surface energy and easier diffusion for both stages. Making the appropriate adjustments to the terms δD_b, D_v, and γ, the model predicts the temperature-density curves for the high oxygen powder very well and the low oxygen powder fairly well as shown in figure 11.

It should be noted that the tuned model was beginning to predict some grain growth potential as indicated by the shaded regions of the sinter map. The tuned model was also predicting that the dominant mechanism responsible for the densification of the compacts was surface tension-controlled volume diffusion. This is evident in the experimental data as well. Note that as the sintering temperature was increased, more porosity was trapped intragranularly (recall figure 3) indicating that volume diffusion is controlling once this stage of sintering is reached. The results from the modeling of the kinetics study were similar. The tuned model agreed fairly well with the experimental data for both oxygen content powder compacts, using the same model parameters for both. Figure 12 shows the model predictions and experimental data for the initial model parameters. Figure 13 shows the effect of tuning on the model predictions. The fact that both predictions were in good agreement for both powders in the kinetics study indicated that the combination of oxygen content and sinter temperature affect the active mechanisms while the time at temperature has a much smaller effect.

A summary of the modifications that were made to the model input parameters is given in Table III. These modifications to the model parameters are certainly not the only appropriate ones to make. A closer match for the low oxygen powder compacts may be achieved by making subtle changes to some of the secondary terms. For example, a modification to the particle radius or maximum to mean particle radius ratio may act in a similar way as the surface energy term, except to a lesser extent. This may be a valid adjustment to the model parameters since the model assumes a spherical particle morphology and a Gaussian size distribution, and in this case the actual powder does not fit those criteria. Additional modifications to the boundary and surface diffusion and energy terms may also serve to provide a better model fit.

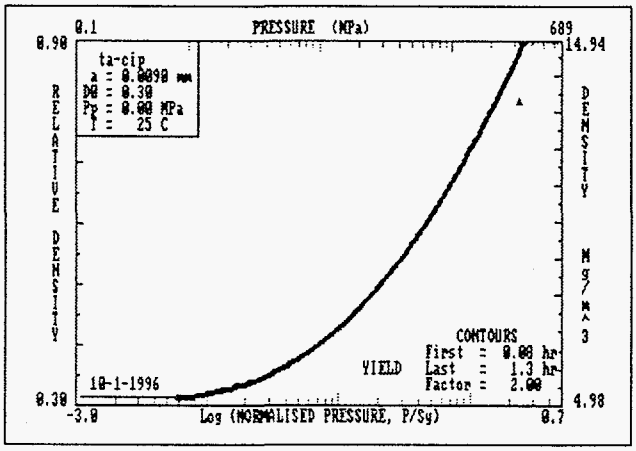

Figure 8. Ashby deformation map for the cold isostatic pressing of tantalum. Untuned.

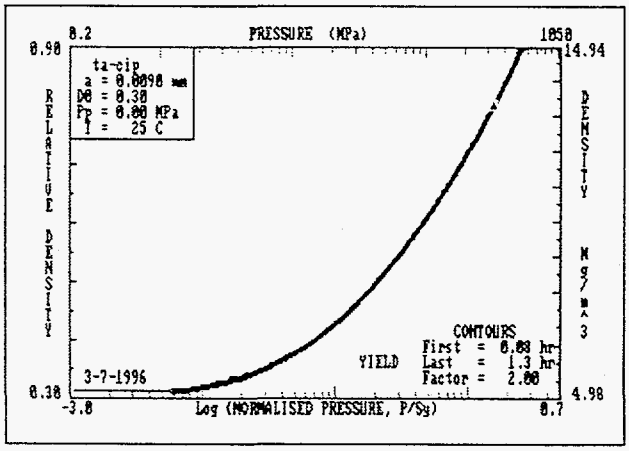

Figure 9. Ashby deformation map for the cold isostatic pressing of tantalum. Tuned.

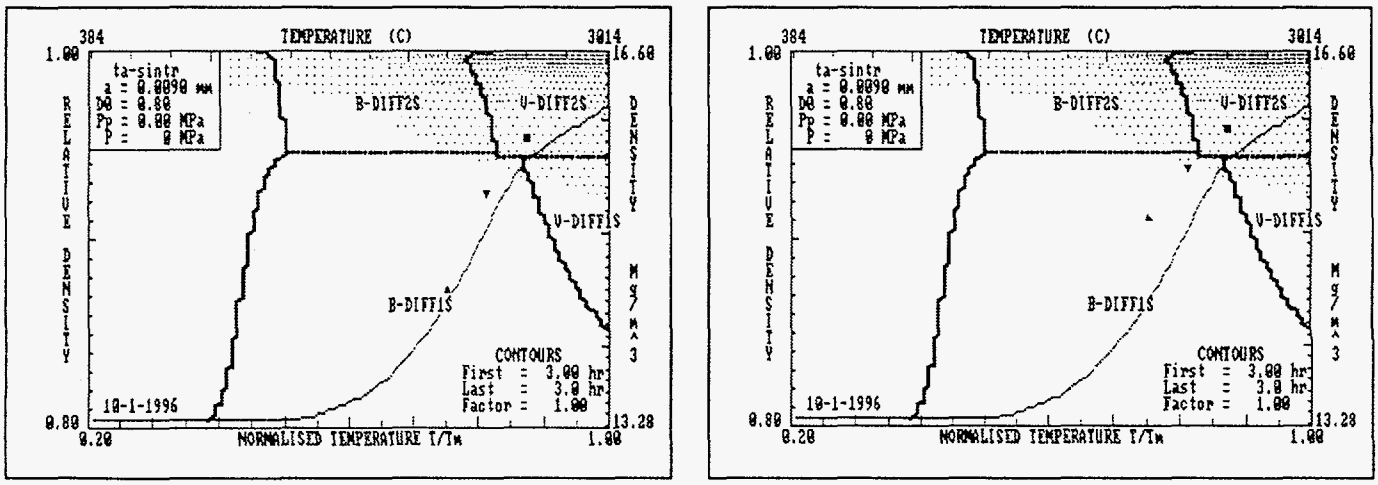

a b

Figure 10. Ashby sinter maps predicting the temperature-density response for a) high oxygen content tantalum, and b) low oxygen content tantalum sintered for 3 hours at temperatures ranging from 2200-2600°C. Untuned.

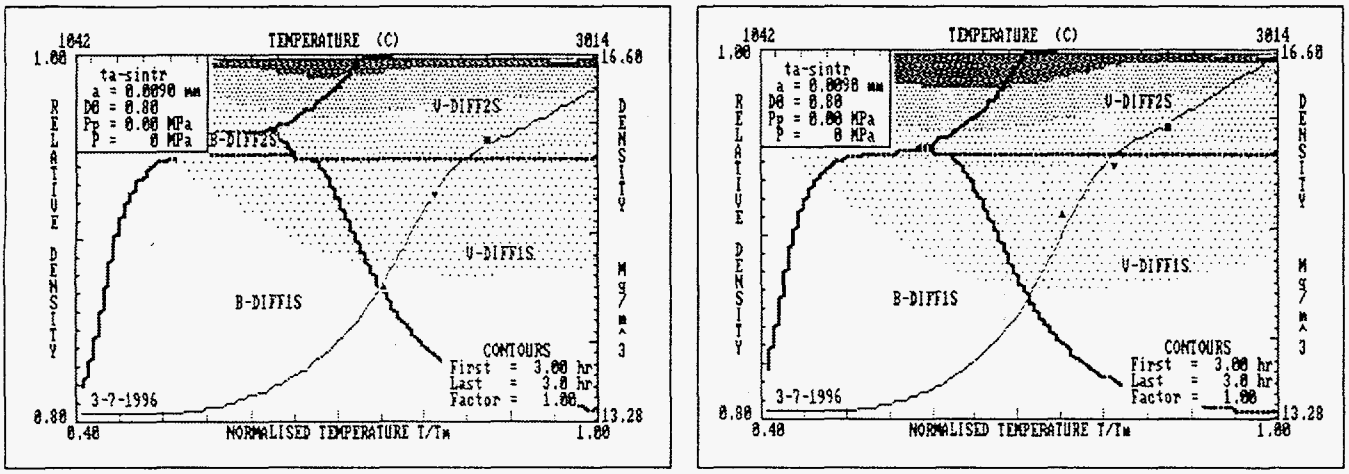

a b

Figure 11. Ashby sinter maps illustrating the effects of tuning the model on the prediction of the temperature-density sintering response of a) high oxygen content Ta, and b) low oxygen content Ta.

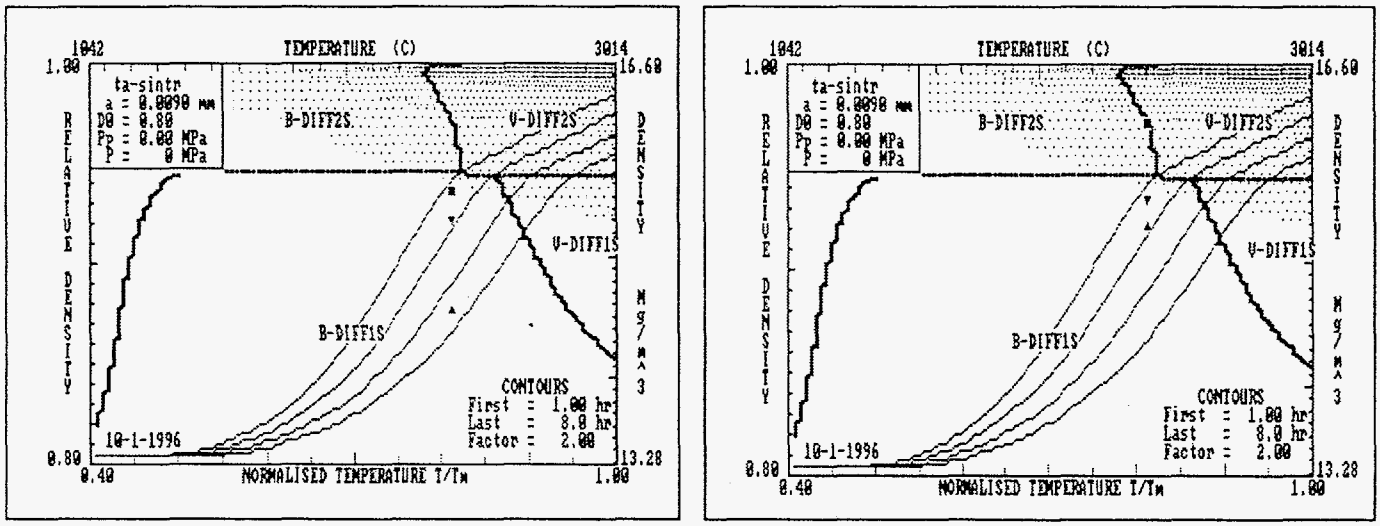

a b

Figure 12. Ashby sintering maps for a) high oxygen and b) low oxygen Ta sintered at constant vacuum and 2400°C for various hold times. Untuned.

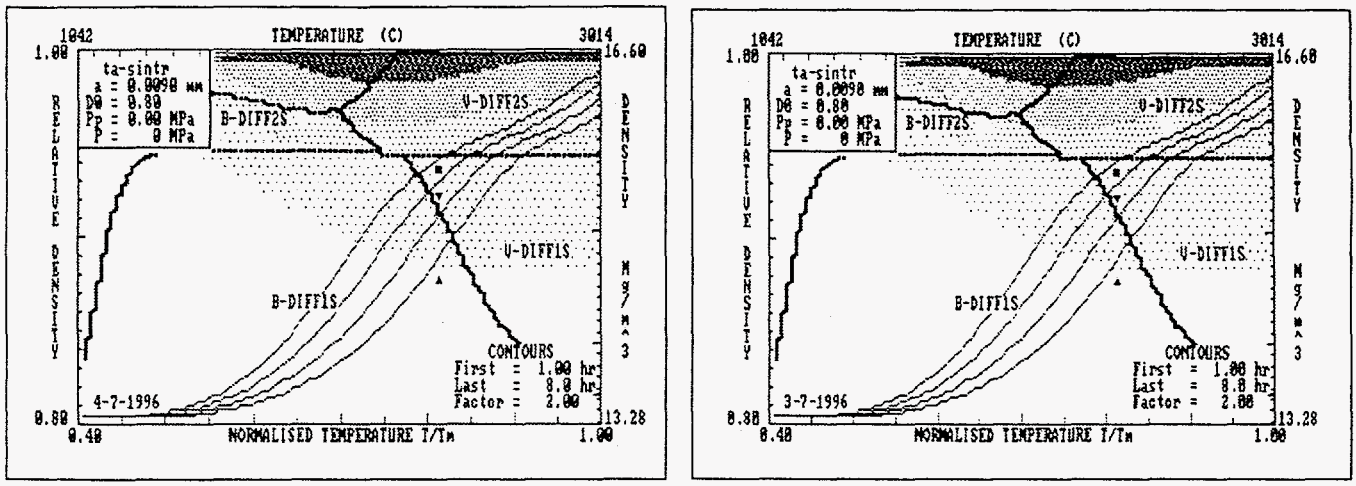

a b

Figure 13. Ashby sintering maps for the kinetics studies showing a) very good agreement between experiment and model for the high oxygen content powder and b) lesser agreement for the low oxygen content powder compacts. Tuned.

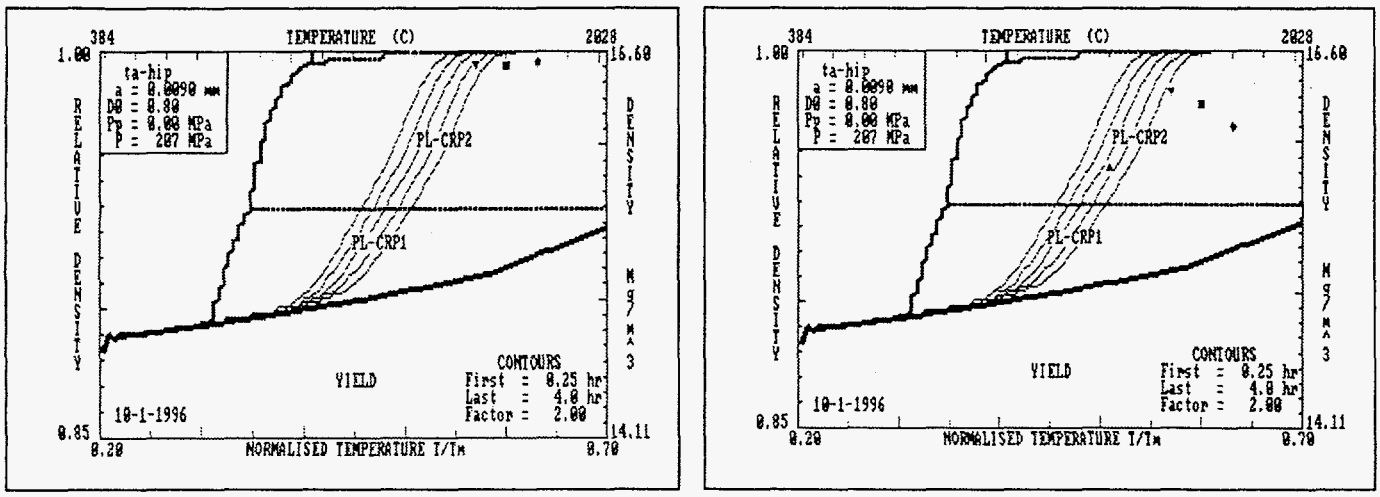

a b

Figure 14. Ashby HIP maps for a) high oxygen and b) low oxygen Ta powders processed at 207 MPa for one hour at temperatures ranging from 1400 to 1800°C. Untuned.

Table III. Initial and modified parameters used in the Ashby model.

Parameter	Initial	High O_2 T-D	Low O_2 T-D	High O_2 Kinetic	Low O_2 Kinetic
Pre-exp. Vol. Diff. (m^2/s)	$1.0X10^{-4}$	$7.0X10^{-4}$	$2.0X10^{-3}$	$5.0X10^{-3}$	$5.0X10^{-3}$
Act. Energy Vol. Diff. (kJ/mol)	491.91	491.91	491.91	550	550
Pre-exp. Bdry. Diff.(m^3/s)	$2.63X10^{-14}$	$2.5X10^{-14}$	$4.0X10^{-14}$	$5.0X10^{-14}$	$5.0X10^{-14}$
Act. Energy Surf. Diff. (kJ/mol)	491.91	425	400	425	425

The untuned model predictions for the hot isostatic pressing of the two powders are shown in figure 14. The model predicts the densification fairly well for both powders using the initially entered parameters. However, it does not predict the grain growth observed experimentally. It is expected that adjusting the surface energy term and the activation energy term for power law creep will allow for a reasonable model fit with the experimental data.

Conclusions

The following conclusions were drawn as a result of these studies.

1. Compact outgassing during vacuum sintering was likely due to the evolution of hydrogen at lower temperatures and oxygen at higher temperatures.
2. Sintered densities were consistently above 90%ρ_{th}, and exceeded 95%ρ_{th} in several instances.

3. Microstructural evidence suggested that at high temperatures and longer hold times, the controlling mechanism responsible for densification shifts from boundary diffusion to volume diffusion.
4. Hot isostatic pressing was successful at producing consistently dense compacts. However, the microstructural evaluation suggested that while high oxygen content powders consolidated to full density, the low oxygen content powders retained a fine uniform distribution of intragranular pores, resulting in a slightly lower density product. This was attributed to the lack of particle surface interstitials whose presence would inhibit boundary migration and allow for more efficient pore closing prior to intragranular pore trapping.
5. General observations on the powder products for both processes were in all cases: the high oxygen powder compacts retained finer grain size distributions than the lower oxygen materials, and grain size increased for high temperatures and longer hold times. HIP'ing consistently resulted in higher density products than static sintering.
6. Mechanical property measurements via compression testing showed that the HIP'ed products demonstrated a higher flow stress than conventional wrought materials for all strain rates tested. Although the sintered product properties were not represented in figure 6, they demonstrated flow characteristics very similar to the wrought plate material. This was probably due to a combination of the decrease in interstitial content during vacuum sintering and the presence of porosity in the compacts.
7. Texture analysis was performed on both HIP and sintered products. Both demonstrated an essentially random texture, which reflect in the mechanical properties being isotropic.
8. The initial model assumptions were reasonable and seemed to predict the densification fairly well for both sintering and hot isostatic pressing.
9. Tuning the model for sintering prediction was successful by modifying the surface energy, boundary and diffusion terms in the model.
10. The Ashby model did a good job of predicting the active/controlling densification mechanisms for the high temperature vacuum sintering process, and was experimentally verified.

Acknowledgments

The authors would like to acknowledge the following for their contributions (all LANL except as noted): Julie Bremser for powder characterization and density measurements, Ann Kelly for metallographic preparation and evaluation, Garth Billings (Thermal Technologies, Astro Division) for performing the sintering studies, Rusty Gray for mechanical testing, and R. Sheldon, S. Wright (TSL), and John Bingert for texture measurements and analysis. The authors would also like to thank the following individuals for their insightful technical discussions: Steve Abeln, John Bingert, Randall German (Penn State University), and P.K. Kumar (Cabot Performance Materials).

References

1. S.I. Wright, G.T. Gray III, and A.D. Rollett, "Textural and Microstructural Gradient Effects on the Mechanical Behavior of a Tantalum Plate," Metallurgical and Materials Transactions A, 25A (May 1994), 1025-1031.

2. S.I. Wright, A.J. Beaudoin, and G.T. Gray III, "Texture Gradient Effects in Tantalum," Material Science Forum, 157-162 (1994), 1695-1700.

3. A.M. Rajendran and R.K. Garrett, Jr., "Effects of Texture and Strain Rate an Flow and Fracture in Pure Tantalum," High Strain Rate Behavior of Refractory Metals and Alloys, eds. R. Asfahani, E. Chen, and A. Crowson (The Metallurgical Society, Warrendale, PA, 1992), 289-302.

4. J.B. Clark et al., "Effect of Processing Variables on Texture and Texture Gradients in Tantalum," Met. Trans. A, 22A (Sept. 1991), 2039-2048.

5. J.B. Clark et al., "Influence of Initial Ingot Breakdown on the Microstructural and Textural Development of High Purity Tantalum," Met. Trans. A, 22A (Dec. 1991), 2959-2968.

6. J.B. Clark et al., "Influence of Transverse Rolling on The Microstructural and Texture Development in Pure Tantalum," Met. Trans. A, 23A (Aug. 1992), 2183-2191.

7. C. Feng, T.K. Chattergee, and L. Ting, "Material Characterization of Tantalum for Different Manufacturing Processes," High Strain Rate Behavior of Refractory Metals and Alloys, eds. R. Asfahani, E. Chen, and A. Crowson (The Metallurgical Society, Warrendale, PA, 1992), 45-58.

8. R.J. Mundekis and J.F. Muller, "Effects of Rolling Schedule and Annealing on the High Strain Rate Behavior of Tantalum," High Strain Rate Behavior of Refractory Metals and Alloys, eds. R. Asfahani, E. Chen, and A. Crowson (The Metallurgical Society, Warrendale, PA, 1992),77-96.

9. "Standard Test Method for Microhardness of Materials", ASTM Designation E384-84, Annual Book of ASTM Standards, Vol. 3.01, (ASTM, Philadelphia, PA, 1984), 654-675.

10. "Standard Method for Determining Average Grain Size", ASTM Designation E112-85, Annual Book of ASTM Standards, Vol. 3.01, (ASTM, Philadelphia, PA, 1987), 403-436.

11. M.F. Ashby, HIP 6.0 Background Reading and Operator Manual, (Engineering Department, Cambridge, U.K., Jan. 1990).

12. R.M. German, Powder Metallurgy Science (Princeton, NJ:Metal Powder Industries Federation, 1984) 273.

13. T. Lyman et al, eds., Metals Handbook, 8th Ed., Vol.1, (Metals Park, OH:ASM, 1961) 1222-1224.

14. G.L. Miller, Tantalum and Niobium, (Academic Press Inc., NY, 1959), 318-323, 396-408, 420, 486-499.